Atg8 Transfer from Atg7 to Atg3: A Distinctive E1-E2 Architecture and Mechanism in the Autophagy Pathway
Asad M. Taherbhoy, Stephen W. Tait, Stephen E. Kaiser, Allison H. Williams, Alan Deng, Amanda Nourse, Michal Hammel, Igor Kurinov, Charles. O. Rock, Douglas R. Green, and Brenda A. Schulman

SUPPLEMENTAL EXPERIMENTAL PROCEDURES

Constructs
　　All constructs were generated by standard molecular techniques and coding regions were verified by automated sequencing at the Hartwell Center for Bioinformatics and Biotechnology at St Jude Children's Research Hospital. Point mutants were generated using QuikChange (Stratagene). Protein expression constructs (detailed below) were designed such that tag removal by either Thrombin or TEV protease leaves 2 extra residues (sequence: Gly-Ser) on the N-termini of proteins. Retroviral constructs expressing mouse Atg7 and mutants were generated by subcloning Atg7 into retroviral expression vector LZRS-IRES-ZEO (Werner et al., 2002) followed by insertion of eGFP (Clonetech) into the BamHI site resulting in the expression of eGFP-Atg7 with a 2-residue Gly-Ser linker between eGFP and Atg7.

Proteins and peptides for X-ray crystallography, SAXS, SEC-MALS, AUC, and ITC
　　Atg7, Atg7^{CTD} and Atg7^{NTD} were expressed as GST-fusions from pGEX-4T1 (GE Lifesciences) by induction with 0.6 mM IPTG overnight at 23°C in BL21 Gold (DE3) cells (Novagen). Atg3, Atg3$^{\Delta FR}$ and Atg3C234only were expressed as GST-fusions from pGEX-4T1 (GE Lifesciences) by induction with 0.6 mM IPTG overnight at 16°C in RIL codon enhanced cells (Stratagene). After glutathione affinity chromatography and thrombin cleavage, proteins were purified to homogeneity by ion exchange and size exclusion chromatography (Superdex-200, GE). Unless otherwise noted, proteins were concentrated and stored at -80°C in buffer containing 20 mM Tris pH 7.6, 150 mM NaCl, and 5 mM DTT. Atg3^{FRpep} (sequence: Ac-SIDDIDELIQDMEIKEE-NH) was synthesized and purified by reversed-phase HPLC by the Hartwell Center for Bioinformatics and Biotechnology at St Jude Children's Research Hospital.

Protein preparation for enzyme, crosslinking, and lipidation assays
　　For enzyme, crosslinking, and lipidation assays, Atg7 constructs were expressed, affinity purified and following tag removal were subjected to size exclusion chromatography. Proteins were concentrated to ≥ 1 mg/mL and stored at -80°C in a final buffer containing 20 mM Tris pH 7.6, 150 mM NaCl and 1 mM DTT. Atg3 for lipidation was prepared as described above. Atg3 variants for pulse-chase assays were expressed as His$_6$-MBP-fusions by induction with 0.6 mM IPTG overnight at 16°C in codon enhanced RIL cells (Stratagene) and purified using nickel affinity chromatography. The tags were cleaved from Atg3 variants with TEV protease, and proteins were further purified by ion exchange chromatography. The Atg3 proteins were then desalted into buffer containing 20 mM Tris pH 7.6, 150 mM NaCl and 1 mM DTT and concentrated to ~30 mg/ml before storage at -80°C.
　　Atg7^{trans} and Atg7^{cis} for use in Atg8 transfer assays and crosslinking experiments were made by by co-expressing GST- and His$_6$- versions of Atg7 and sequential pulldowns on the two tags. Atg7^{trans} initially consisted of GST-Atg7(P283D) and His$_6$-Atg7(C507A) and was expressed in BL21 Gold (DE3) cells by induction with 0.6 mM IPTG overnight at 23°C. Atg7^{cis} protein was prepared by coexpressing GST-Atg7(P283D,

C507A) with His$_6$-Atg7 in codon enhanced Rosetta cells (Novagen). Cells were lysed and subjected to sequential nickel and glutathione sepharose affinity chromatography. GST and His$_6$ tags were then cleaved with Thrombin and TEV proteases, respectively. Cleaved proteins were purified by size exclusion chromatography using a Superdex-200 column equilibrated with 20 mM Tris pH 7.6, 150 mM NaCl and 1 mM DTT. The protein was concentrated to ~1 mg/ml and stored at -80°C.

GST-Atg8 corresponding to the ligatable, processed sequence was expressed from the pGEX-2TK vector (GE), which leaves an N-terminal PKA site for radiolabeling after thrombin cleavage of GST. This Atg8 was expressed in Rosetta cells (Novagen) induced with 0.6 mM IPTG overnight at 16°C. After GST purification and thrombin cleavage, Atg8 was purified by ion exchange and size-exclusion chromatography using a Superdex-200 column. Protein was concentrated to ~ 6 mg/mL and stored at -80°C in a final buffer containing 25 mM Tris pH 7.6, 150 mM NaCl and 1 mM DTT.

Analytical Ultracentrifugation (AUC)

Prior to AUC, all proteins were repurified by size exclusion chromatography using a Superdex-200 column equilibrated with 50 mM Tris pH 7.6, 150 mM NaCl, 1 mM DTT. Sedimentation velocity ultracentrifugation experiments were performed in a ProteomeLab XL-I analytical ultracentrifuge with a Beckman An-60 Ti rotor and cells containing sapphire windows and charcoal-filled Epon double-sector centerpieces (Beckman Coulter, Fullerton, CA). Velocity data analysis was performed in SEDFIT using the model for continuous sedimentation coefficient distribution c(s) with deconvolution of diffusional effects (Schuck, 2000; Schuck et al., 2002). Molecular weight of the proteins was calculated based on its amino acid composition using the software SEDNTERP (http://www.jphilo.mailway.com). Sedimentation equilibrium experiments were performed with a Beckman An-50 Ti rotor and quartz windows. Equilibrium was attained at 24 hours at a rotor temperature of 4 °C at increasing speeds of 12, 18, and 22 k rpm for Atg7 and Atg7^{CTD} and 18, 27 and 34 k rpm for Atg7^{NTD}. Proteins at concentrations of between 0.86 and 3.5 μM (120 μL) were loaded into double-sector centrepieces and absorbance distributions recorded at 280 nm in 0.001 cm radial intervals with 20 replicates for each point. Global least squares modeling was performed for data from multiple rotor speeds with the software SEDPHAT (www.analyticalultracentrifugation.com) using a reversible monomer-dimer self-association model (Vistica et al., 2004).

Pull-down assays

Thrombin cleavable GST-Atg7^{NTD} in pGEX4T1 (GE Lifesciences) and TEV cleavable His$_6$-MBP-Atg3 constructs in pRSFDuet (Novagen) were co-expressed in BL21 Gold (DE3) cells by induction with 0.6 mM IPTG overnight at 23°C. Cells were lysed in phosphate-buffered saline at pH 7.4 supplemented with 10 mM Imidazole, 5 mM BME and 2.5 mM PMSF. Clarified lysates were split and subjected to glutathione affinity chromatography and nickel affinity chromatography. Beads were washed and affinity captured protein was eluted using 50 mM Tris pH 8.0, 200 mM NaCl, 5 mM DTT and 10 mM reduced glutathione or PBS pH 7.4 supplemented with 250 mM Imidazole and 5 mM BME, for GST- and His$_6$-pulldowns, respectively, and analyzed by SDS-PAGE. In the event that protein bands for GST-Atg7^{NTD} and His$_6$-MBP-Atg3 constructs co-migrated on gels, cleavage with thrombin distinguished them.

***In vitro* assay of Atg7~Atg8 thiolester formation**

Atg7 and Atg8 proteins were reduced by addition of 10 mM DTT then desalted once over Zeba desalting columns (Pierce). Reactions containing 1 μM Atg7 and 2 μM Atg8 in 50 mM HEPES pH 7.5, 50 mM NaCl, 1 mM MgCl$_2$, 1 mM ATP were incubated at room temperature for 90 seconds then quenched by addition of SDS sample buffer (non-

reducing). Formation of the thiolester intermediate was verified by side-by-side SDS-PAGE analysis under reducing conditions.

In vitro Atg8~PE Conjugation Assay

Lipidation assays were performed essentially as outlined (Ichimura et al., 2004; Nakatogawa et al., 2007). Atg8 was prepared as described for the pulse-chase assay above, except that it was expressed from the pGEX-4T1 vector (GE). "Atg12~5" in the main text refers to an optimized version previously described to contain Atg12 residues 100-186 and Atg5 residues 1-284 based on structural studies (Noda et al., 2008a). To generate this complex, His_6-Atg12 (residues 100-186) and untagged Atg5 (residues 1-284) were coexpressed from pRSF-DUET along with untagged Atg7 and Atg10 expressed from pET-DUET. Protein expression was induced with 0.6 mM IPTG overnight at 19°C in BL21 Gold (DE3) cells. After nickel affinity chromatography the His-tagged Atg12(100-186)~5(1-284) conjugate was further purified by size exclusion chromatography (Superdex S200, GE) in 20 mM HEPES 7.2, 150 mM NaCl, 0.2 mM DTT. Contaminating *E. coli* nickel-binding Crp and SlyD proteins (Bolanos-Garcia and Davies, 2006) were identified by mass spectrometry (Hartwell Center for Bioinformatics and Biotechnology). Liposomes were prepared by mixing POPC (1-palmitoyl-2-oleoyl-phosphatidylcholine), DOPE (dioleoyl-phosphatidylethanolamine) and DOPG (1,2-dioleoyl-phosphatidylglycerol) dissolved in chloroform and drying under nitrogen. Lipids were hydrated in 20 mM HEPES 7.2 for 60 minutes at 37°C with periodic vortexing, then placed in bath sonicator for 5 min, and extruded (12 times) with a microextruder through a 400 nm polycarbonate filter (Avanti). Liposomes composed of 60% POPC, 25% DOPE, 15% DOPG were added to a final concentration of 350 μM in reactions containing 200 nM Atg7 (wild-type or mutants), 500 nM Atg3, 5 μM Atg8, 1.6 μM His_6-Atg12(100-186)~Atg5(1-284) (Noda et al., 2008a), 50 mM Tris 8.0, 100 mM NaCl, 2 mM ATP, 5 mM $MgCl_2$. At the indicated times, reactions were quenched by adding an equal volume of SDS loading buffer containing 3 M urea and 100 mM DTT, and analyzed on 13.5% PAGE gels containing 6 M urea.

Small-angle X-ray scattering (SAXS)

SAXS data were collected at the ALS SIBYLS beamline 12.3.1, Berkeley, CA using a wavelength (λ) of 1.0 Å and sample-to-detector distances set to 1.5 m, resulting in scattering vectors, q, ranging from 0.01 Å^{-1} to 0.32 Å^{-1}. The scattering vector q is defined as $4\pi \sin\theta/\lambda$, where 2θ is the scattering angle. Experiments were performed at 20°C and the data were processed as described (Hura et al., 2009). Data acquired for short and long exposures (0.5 and 5 s) were merged for calculations using the entire scattering profile. The SAXS profiles and corresponding fits to the experimental data were calculated using the program FoXS (Schneidman-Duhovny et al., 2010). The experimental SAXS data for different protein concentrations (Atg7^{CTD} at 3.3, 2.5 and 1.65 mg/ml; Atg7 at 1.2 and 0.25 mg/ml) were investigated for aggregation using Guinier plots. The inset panel in Figure 6 shows the Guinier plots (magenta line) for the merged datasets. The radius of gyration R_G of 31.2 ± 0.1 Å for Atg7^{CTD} and 49.5 ± 0.5 Å for Atg7 were derived by the Guinier approximation with the limits qR_G=1.6 (Guinier and Fournet, 1955).

Size Exclusion Chromatography Multi-angle Light Scattering (SEC-MALS)

The stoichiometry of a cross-linked Atg7~BMOE~Atg3C234only complex purified by size exclusion chromatography (Superdex S200) was analyzed by Size Exclusion Chromatography (Shodex KW-804) coupled to in-line Multi-Angle Light Scattering (SEC-MALS) (Wyatt DAWN HELEOS) with in-line refractive index detection (Wyatt Optilab rEX). The wavelength used was 658 nm and the calibration constant was 2.32950e-4 1/(V cm). The column was equilibrated with 25 mM HEPES pH 7.0, 150 mM NaCl, 2 mM DTT and experiments were conducted at 25 °C. The injected sample volume was 30 μl and

experiments were conducted at a flow rate of 0.5 ml/min. The size-exclusion limit of the column was 500 kDa, and protein was loaded at 0.19 mg/ml. Eluted protein was detected via light scattering and refractive index and data were recorded and analysed with Wyatt Astra software (version 5.3.4). The refractive index increment, dn/dc, was assumed to be 0.185 ml/g.


Cell-based assays

Cells were cultured in DMEM supplemented with 10% FCS, 1 mM pyruvate, 1 mM glutamine, 100 U/mL penicillin, 100 mg/mL streptomycin in a humidified environment at 37^0C with 5 % CO_2. Phoenix Eco cells (provided by Garry Nolan, Stanford University) were transfected with LZRS GFP-Atg7 retroviral constructs using Lipofectamine 2000 (Invitrogen). Two-days post transfection, viral supernatant was harvested, filtered through a 0.2 mM filter and polybrene was added to 5 mg/ml final concentration. To generate Atg7 null murine embryonic fibroblasts (MEF) cell lines, timed matings of Atg7 +/- mice were setup (Sanjuan et al., 2007). At day E12, embryos were removed and primary MEFs were isolated. Atg7 null MEFs were identified by genotyping and transformed with SV40 plasmid (gift from J. Opferman, St. Jude Children's Research Hospital). SV40 transformed, Atg7 null MEFs (1 x10^5 cells per well of a 6 well dish) were infected with viral supernatant. Two days post-infection, transduced cells were selected using Zeocin (100 mg/ml, Invitrogen). To ensure equal expression of wild-type and mutant GFP-Atg7 fusion proteins, the stably transduced polyclonal cell lines were sorted once by flow cytometry using an identical sort gate.

Cells were lysed on ice for 30 minutes in NP40 lysis buffer (1% NP40, 150 mM NaCl, 1 mM PMSF, Complete protease inhibitors (Roche)). Lysates were clarified by centrifugation at 10,000 g for 10 minutes at 4^0C, assayed for total protein content using Biorad protein assay, separated by SDS-PAGE and transferred to nitrocellulose for immunoblotting with primary antibodies against LC3 (Cell Signaling catalog #2775), Atg12 (Cell Signaling catalog #2011S), Atg7 (Sigma catalog #A2856) and GAPDH (Millipore catalog #MAB374). HRP-conjugated secondary antibodies were detected by Supersignal ECL (ThermoScientific).

Modeling Atg8 transfer

For simplification, to build a model for transthiolation, only one of the two Atg7 protomers from the asymmetric best-fit SAXS model was used as a template. Atg3 (PDB code: 2DYT) (Yamada et al., 2007) missing the FR region, was manually aligned with its catalytic Cys in close proximity to the Atg7 catalytic Cys. The Atg7[NTD]-Atg3[FRpep] structure was aligned to the model using SSM Superpose in Coot (Emsley et al., 2010), and within reasonable distances to their connections in the remainder of Atg7 and Atg3, respectively. Next, using SSM Superpose in Coot (Emsley et al., 2010), the MoeB-MoaD structure [PDB code: 1JW9 (Lake et al., 2001)] was aligned with the Atg7[CTD] in the model, and Atg8 [PDB code: 2ZPN (Noda et al., 2008b)] was superimposed onto MoaD. Since the C-terminal tail of Atg8 was absent in the crystal structure, we used the corresponding tail region from MoaD (Lake et al., 2001) and appended it to the Atg8 structure. Finally the C-terminal tail was rotated to contact Atg7's catalytic cysteine to represent Atg8 thiolester bound to Atg7.

A

	α7	α8	β16	α9	β17	α10	β18	
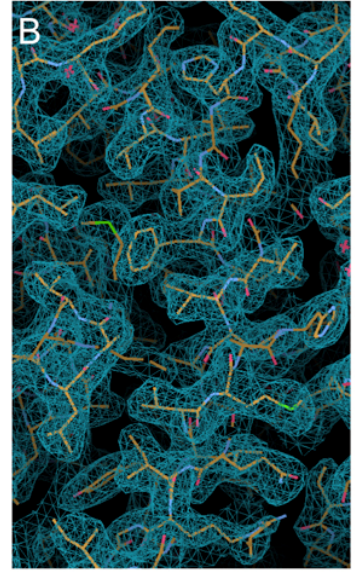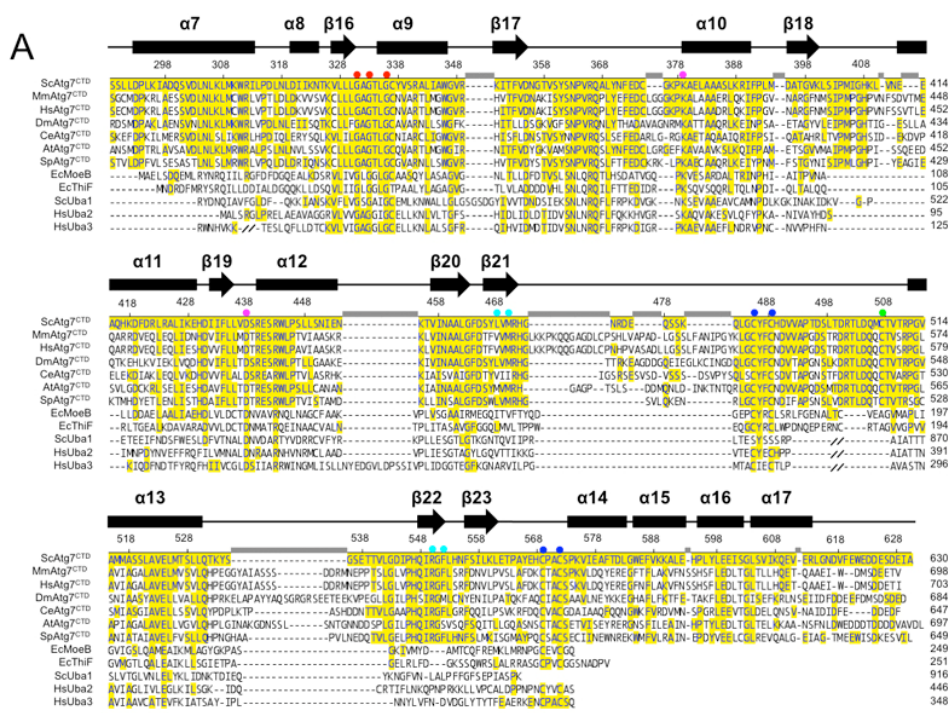
→ Strand   ▬ Helix   ● MgATP binding   ● Atg8 binding

● G-X-G-X-X-G nucleotide binding motif   ● Zn coordinating cysteines   ● Atg7 catalytic cysteine

C

K379   D438
ATP

Atg7^{CTD} conservation with other E1s

0% 100%

D

F552
R550
L468
M470
K379   D438
ATP
Atg8

Atg7^{CTD} conservation across species

0% 100%

E

Atg7: WT C507A R550A,F552A L468A,M470A K379A D438A

Atg7~Atg8 →
Atg7 →
-DTT

Atg8 Binding   MgATP Binding

Atg7: WT C507A R550A,F552A L468A,M470A K379A D438A

Atg7 →
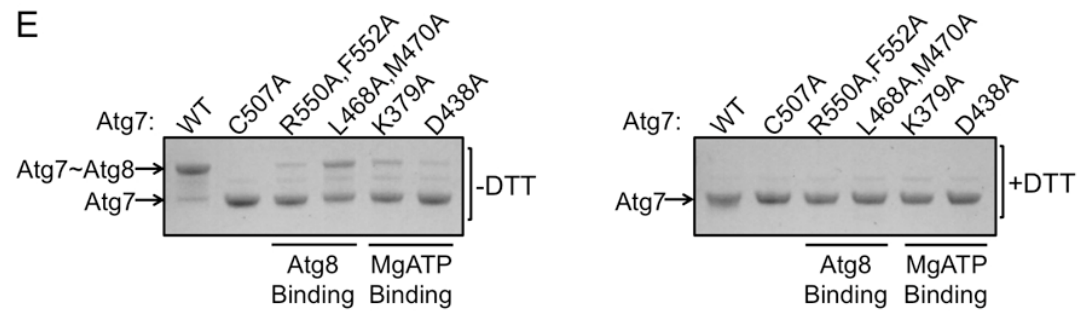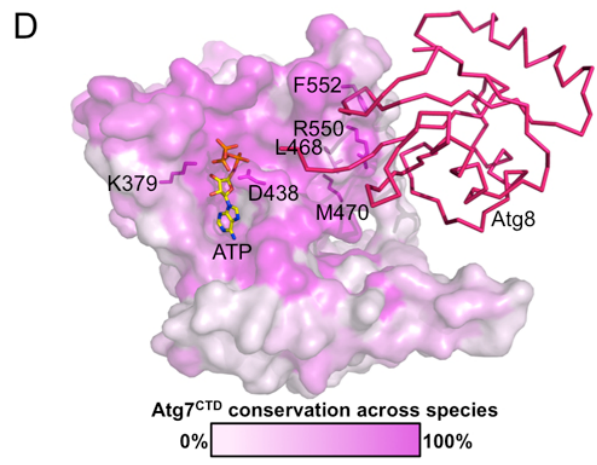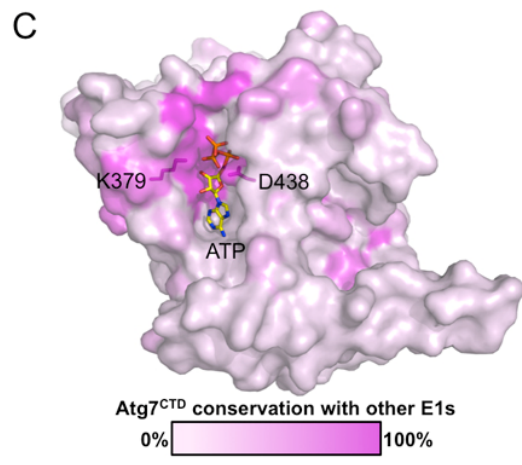+DTT

Atg8 Binding   MgATP Binding

Figure S1. Structural Features of Atg7^{CTD}

(A) Sequence alignment of *Saccharomyces cerevisiae* Atg7^{CTD} (Sc) with corresponding regions of Atg7 from mouse (Mm), human (Hs), *Drosophila melanogaster* (Dm), *Caenorhabditis elegans* (Ce), *Arabidopsis thaliana* (At) and *Schizosaccharomyces pombe* (Sp), *Escherichia coli* (Ec) MoeB, Ec ThiF, Sc Uba1, Hs Uba2 and Hs Uba3. Secondary structures and some functional residues are indicated above the alignment. Double slash is in place of N-terminal residues and insertions not included in the alignment.

(B) Final 2F$_o$-F$_c$ electron density map contoured at 1σ (blue) over a region of Atg7^{CTD}.

(C) Conservation between *S. cerevisiae* Atg7^{CTD}, *E. coli* MoeB and ThiF, *S. cerevisiae* Uba1, and human Uba2 and Uba3 displayed on a semi-transparent surface over the Atg7^{CTD} crystal structure. White - 0 conservation; magenta - 100% conservation. ATP is modeled based on superimposing the MoeB-MoaD-ATP structure (Lake et al., 2001). Side-chains of conserved MgATP binding residues Lys379 and Asp438 are shown in sticks.

(D) Conservation among *S. cerevisiae*, mouse, human, *D. melanogaster*, *C. elegans*, *A. thaliana* and *S. pombe* Atg7s displayed on a semi-transparent surface over the Atg7^{CTD} crystal structure. White - 0 conservation; magenta - 100% conservation. For clarity, the Cys-loop was omitted from the structure owing to its masking visualization of the β-sheet. ATP is modeled based on superimposing the MoeB-MoaD-ATP structure (Lake et al., 2001). Atg8 (Noda et al., 2008b) is modeled based on its subsequent superimposition with MoaD, with the C-terminal tail taken from the MoaD structure. Side-chains of conserved MgATP and UBL binding residues Lys379 and Asp438, as well as Leu468, Met470, Arg550, and Phe552 in the predicted Atg8-binding surface are shown in sticks.

(E) Coomassie-stained SDS-PAGE gel showing formation of the thiolester-linked Atg7~Atg8 complex by wild-type (WT) Atg7 or the indicated mutants in the catalytic Cys (C507) or predicted Atg8 or MgATP binding surfaces. Formation of a thiolester bond under these conditions was confirmed by collapsing down to the Atg7 only band upon treatment with DTT.
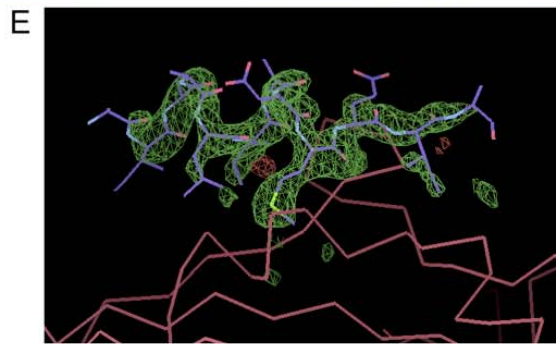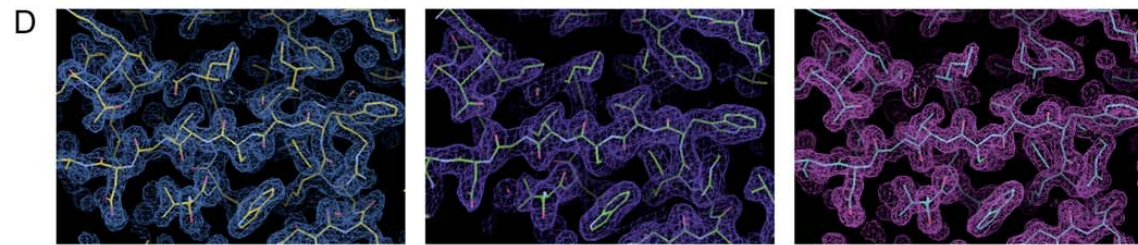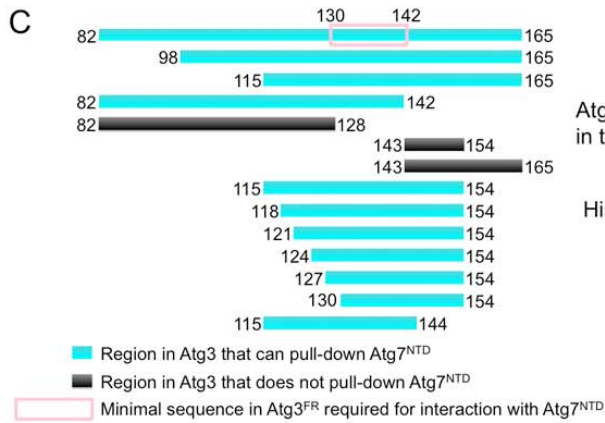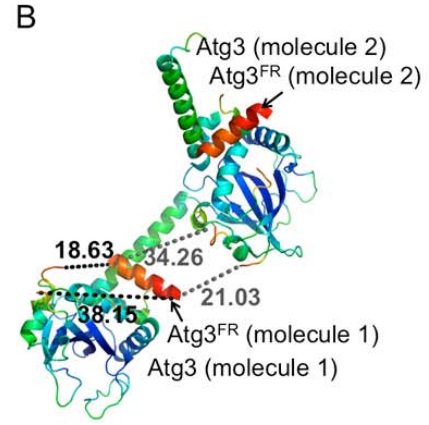
A

β1 α1 β2 β3 β4 α2

ScAtg7NTD	MSSERVLSYAPAFKSFLDTSFFQELSRLKLDVLKLDSTCQPLTVNLDLHNIPKSADQVPLFLTNRSFEKHNNKR	98
MmAtg7NTD	----MGDPGLAKLQFAP--FNSALDVGFWHELTQKKLNEYRLDEAPKDIKGYYYNGDSAGLPTRLTLEFSAFOMSASTPAH------------CCPAMGTLHNTNTLEAFKTADK	97
HsAtg7NTD	MAAATGDPGLSKLQFAP--FSSALDVGFWHELTQKKLNEYRLDEAPKDIKGYYYNGDSAGLPARLTLEFSAFOMSAPTPAR------------CCPAIGTLYNTNTLEFKALDK	101
DmAtg7NTD	----MSTEKEIILQFAP--WESFVSPTFWHKLAELKLNEYRLDSDSKRSITGHYTNRNASG--CLLEVDYTAYNRMAKPPK------------FSHSAIGTIYNKNTIEEFKALDK	95
CeAtg7NTD	---------MATFVP--FVTCLDTGFWHEVNKKKLNDWKLDEIPKCISSQLSLHQTEGFKCHLSLSYDSLSESTTG--------------------LSMSGTLLLYNTIESFKMVDK	88
AtAtg7NTD	---MAEKETPAIILQFAP--LNSSVDEGFWHSFSSLKLKLDHGKLGIODSPISIYGFYGPCGHPQVSNHLTLLSESLPLDEQSLIASTSHGNRNKCPVPGILYNTNTVESFNKLDK	107
SpAtg7NTD	----MFVGKALQFQS-FHSSIDATPVHQLSLVVKVEKQKLDSPLTIHGKFNTY-SRQN--ISIVFGEAPSNSNIKD------------CLAEGTLLNANTPQEFTNADV	89

α3 β5 β6 β7 β8 α4 β9 β10

ScAtg7NTD	QLFLHQRALECWEDG------IKDINKCVSFVIISFADLKKYRFYYNLGVSPCFQR-RS---------------STVLHVRPEPSLKGLFSKCQKWFDVNYSKWVCILDADDEIVN	191
MmAtg7NTD	KLLLEQSANEIWEAIKSGGAALENPMLLNKFLLTFADLKKYHFYYWFCCPALCL-PESIPLIRGPVSLDQRLSPKQIQALEHAYDDLCRAEGVTALPYFLFKYDODTVLV	206
HsAtg7NTD	KLLLEQAANEIWESIKSGTALENPVLLNKFLLTFADLKKYHFYYWFCCPALCL-PESLPLIQGPVGLDQRFSLKQIEALECAYDNLCQTEGVTALPYFLKYDENMVLV	210
DmAtg7NTD	LQLLADEGKELLADMCSGGALRDLTRRFFVLSSLTRFFIIAFADLKKCHSYYYWFAFPCPLT-PT-------LKLQGAVQKLRDLPNSSSYIMALKALPTESQNFFILYANVEKNIFE	197
CeAtg7NTD	SDLIRSEAEKIWESITTRKWLQNPRLLSSQFFIIAFADLKFKYYWTCVPALVY-PS----------EIKQEITPLSSLGADHKILFDFYRKNFPIFLYSKQSSKMLE	186
AtAtg7NTD	QSLLKLAEANKIWEDIQSGEALEDFWHSFSSLKLKLDHGKLGIODSPISIYGFYGPCGHPQVSNHLTLLSESLPLDEQSLIASTSHGNRNKCPVPGILYNTNTVESFNKLDK	289
SpAtg7NTD	KKIREEIGEVLLSNIKNGVVSERPNELLRFLIFSYADIKAYKYHYWCLFPSFKETP-----HWIWKDLSPAESLIPSGPILSQIREFLSTADYYQRPFFLLIKSTLDEWT	194

α5 β11 α6 β12 β13 β14 β15

ScAtg7NTD	YDKCIIR------KTKCVLAIRDTSTMENVPSALTKNFLSVLQYDVP-DLIDFKLLIIRQNEGSFALNAT--FASIDPQSSSSNPDMKVSGWERNVQGKLAPRVVDLS	289
MmAtg7NTD	SLLLHKYSDFFQGQRTKITVGVYDPCNLAQYPGWPLRNFLVLAAHRWSGSFQSVEVLCFRDRTMQGARDVTHSIIFEVKLPEMAFSPDCPKLAVGGWENKNQKGQGMQPRMWLCMR	316
HsAtg7NTD	SLLLKHYSDFFQGQRTKITIGVYDPCNLAQYPGWPLRNFLVLAAHRWSGSFQSVEVVCFRDRTMQGARDVAHSIIFEVKLPEMAFSPDCPKLAVGGWENKNQKGQGMQPRMWLCMR	320
DmAtg7NTD	ARSLSSLD--DKNVEFCYFGDPSEY-EHPAWIMRNYAAFLLQQCPSFVGKPLKFLGLRHNQQMNIDDSLVWKVIQTEACDLSGSENIKFGGWELNKNGKNQGMQPRMWCMR	304
CeAtg7NTD	LSELEN-----NTNPDEICVVVADPSPVAYSAGWMWRNVLAAVAHLHP--TWKHCHIISLRSADSIGIKYTWT--LPSAECSADGAQNAVPKAVGGWENKNNANDKLLQPISVDLS	289
AtAtg7NTD	IRHLKDLEACQGDHQKLLFGFYDPCHLPSNGPGWPLRNYLALIRSRWN---LETVWFFCYRESRGFALTNLSLVGQASITLSSGESAETVPNSVGWELN--KGKRVPRSISLA	322
SpAtg7NTD	IAPLKELSHCVDKSLQFYLVAEDSVQLAEYPSWPVRNILAFAFIKFK---LKVINLFLYRDGINSDTLSKSI--LIKVEADKDMILEAPLSIVGGWERNGKVLGPRVVNLS	300

➤ Strand ▬ Helix ● Atg3FR binding

B

C

Atg3 residues used in the pull-down:

82-165 98-165 115-165 82-142 82-128 143-165 143-162 115-154 118-154 121-154 124-154 127-154 130-154 115-144

His6-MBP-Atg3FR [
Atg7NTD →
GST →

■ Region in Atg3 that can pull-down Atg7NTD
■ Region in Atg3 that does not pull-down Atg7NTD
▭ Minimal sequence in Atg3FR required for interaction with Atg7NTD
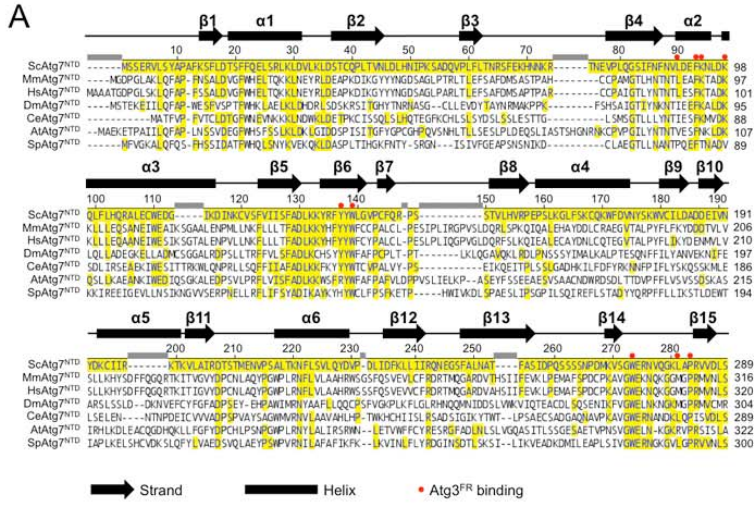
D

E

Figure S2. Atg3^{FR} Interactions with Atg7^{NTD}

(A) Sequence alignment of *S. cerevisiae* Atg7^{NTD} (Sc) with corresponding regions of Atg7 from mouse (Mm), human (Hs), *D. melanogaster* (Dm), *C. elegans* (Ce), *A. thaliana* (At) and *S. pombe* (Sp). Secondary structure assignment is based on the structure of yeast Atg7^{NTD} described in Fig S3.

(B) A prior structure of *S. cerevisiae* Atg3 (Yamada et al., 2007) is shown, with two symmetry-related molecules of Atg3 (PDB code: 2DYT) colored by C-α B-factors, with regions in red having the highest B-factors and regions in blue having the lowest B-factors. Distance between Atg3^{FR} of molecule 1 with the core Atg3 of molecule 1 is shown in black (total measured distance is 56.78Å). Distance between Atg3^{FR} of molecule 1 with the core Atg3 of molecule 2 is shown in grey (total measured distance is 55.29Å). It is not clear whether the Atg3^{FR} in the prior crystal is part of the same molecule it packs against, or is from an adjacent Atg3 molecule in the crystal.

(C) Schematic and gel showing truncations of *S. cerevisiae* Atg3^{FR} analyzed in a pull-down assay with wild-type Atg7^{NTD} and Atg3^{FR} fragments coexpressed in E. coli. Numbers above the gel panel correspond to the residues within Atg3 that were used in that pull-down.

(D) Final 2F$_o$-F$_c$ electron density map contoured at 1σ (blue) over a region of Atg7^{NTD} (left), over a region of Atg7^{NTD} from the Atg7^{NTD}-Atg3^{FRpep} complex (center), and over a region of Atg7^{NTD}(P283D) (right).

(E) F$_o$-F$_c$ difference map contoured at 3σ (green) over the Atg3^{FRpep} (purple). The map was generated by performing simulated annealing starting at 4000 K, in 500 cooling steps to a final 300 K without the peptide present using PHENIX (Adams et al., 2010). The backbone Cα trace of Atg7^{NTD} is displayed red.
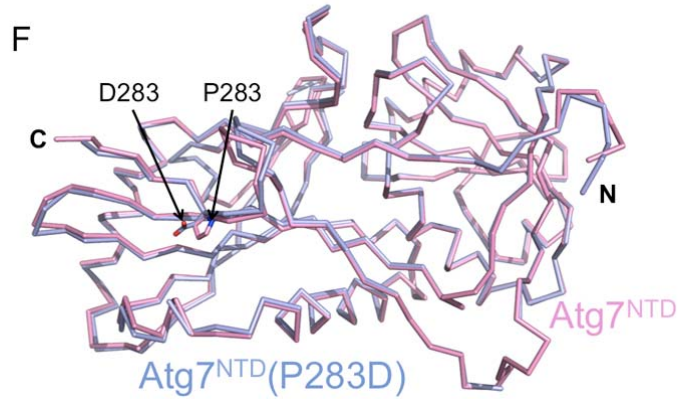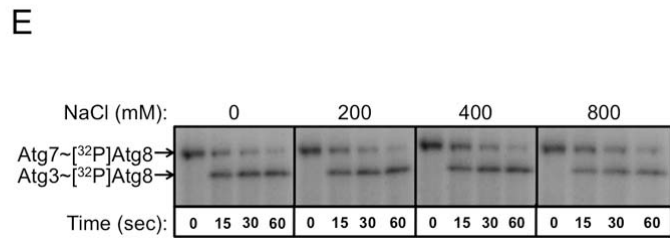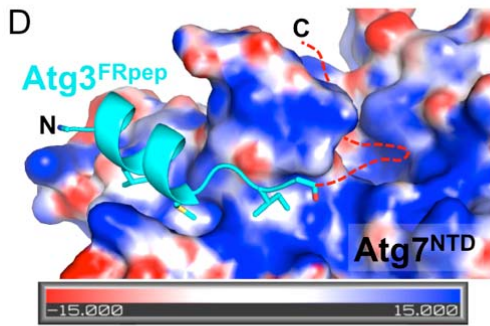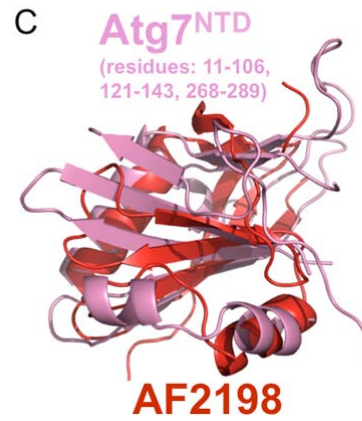
A

Atg7^{NTD}

B
Atg7^{NTD}
(residues: 11-106, 121-143, 268-289)

Atg7^{NTD}
(residues: 1-10, 144-267)

C
Atg7^{NTD}
(residues: 11-106, 121-143, 268-289)

AF2198

D
Atg3^{FRpep}
Atg7^{NTD}

E
NaCl (mM): 0   200   400   800
Atg7~[³²P]Atg8
Atg3~[³²P]Atg8
Time (sec): 0 15 30 60   0 15 30 60   0 15 30 60   0 15 30 60

F
D283   P283
Atg7^{NTD}
Atg7^{NTD}(P283D)
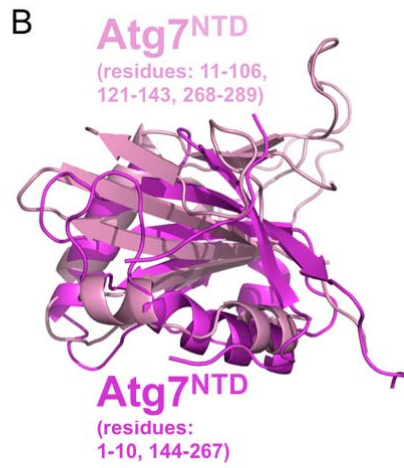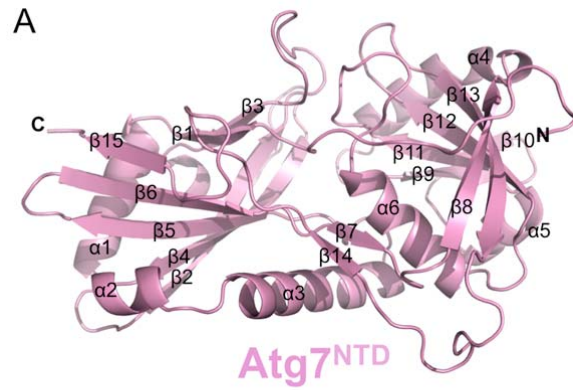
Figure S3. Structural Features of Atg7^{NTD}

(A) Structure of Atg7^{NTD} with strands and helices numbered.

(B) Overlay of the two subdomains of Atg7^{NTD}: Residues 11-106, 121-143 and 268-289 from the Atg7^{NTD} structure (pink) overlaid with residues 1-10 and 144-267 from the Atg7^{NTD} structure (magenta).

(C) A search for homologous structures using the DALI server (Holm and Rosenstrom, 2010) identified several proteins having an MPN (Mpr1, Pad1 N-terminal) fold. MPN domains are thought to mediate protein-protein interactions, and also with the appropriate constellation of zinc ligands form hydrolases such as cytidine deaminases and AMSH-LP in the JAMM-family deubiquitinating enzymes (DUBs) (Pena et al., 2007; Sanches et al., 2007; Sato et al., 2008; Tran et al., 2003). However, we cannot speculate as to any functional significance of this structural homology, as Atg7^{NTD} lacks numerous features associated with zinc and UBL-binding by JAMM DUBs, and the UBL surface corresponding to the region of ubiquitin recognized by JAMM-family DUBs would presumably be sequestered upon Atg8 binding to the Atg7^{CTD}. Structural similarity is shown by overlay of residues 11-106, 121-143 and 268-289 from the Atg7^{NTD} structure (pink) with the structure of *Archaeoglobus fulgidus* AF2198 JAB1/MPN domain protein (red) (PDB: 1OI0) (Tran et al., 2003).

(D) Atg7^{NTD} is displayed in surface representation with the electrostatic potential (calculated using APBS (Baker et al., 2001)) shown. Atg3^{FRpep} is shown as cartoon with key side chains displayed as sticks. Red dashes represent the approximated trajectory of the polyacidic stretch of Atg3's FR following the Atg3^{FRpep} sequence.

(E) Autoradiogram showing time course of the transfer of [^{32}P]Atg8 from Atg7 to Atg3 (transthiolation reaction) under increasing salt concentrations.

(F) Crystal structures of Atg7^{NTD} (pink) and Atg7^{NTD}(P283D) (blue) superimpose with a 0.55 Å root-mean-square deviation.
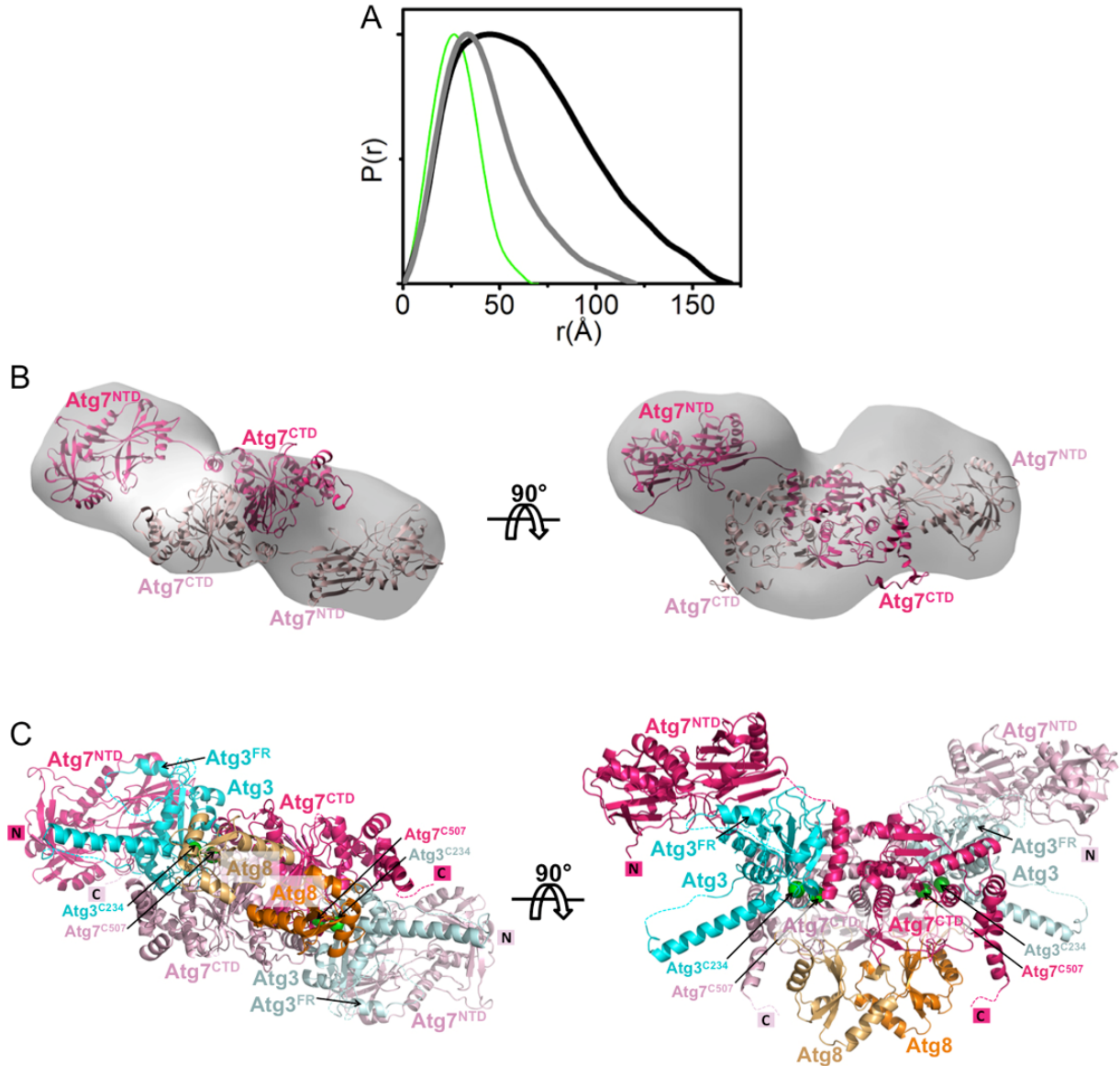
Figure S4. A "trans" Mechanism for Transthiolation

(A) Experimental Pair-distribution function (P(r)) of Atg7 (black), Atg7^{CTD} (gray), and reference theoretical P(r) for a hypothetical Atg7^{CTD} monomer (green).

(B) Two views of the Atg7 model used to calculate the theoretical scattering profile (Fig. 6A) generated using BILBOMD (Pelikan et al., 2009). Atg7 residues 289-293 were defined as being flexible to optimize the position of the N-terminal domain. The best fit model (χ^2=1.5) was superimposed on the average SAXS shape reconstruct by DAMMIF (Franke and Svergun, 2009).

(C) Model for transthiolation reaction containing dimeric Atg7 bound to two Atg3s and two Atg8s, as described in Supplemental Experimental Procedures. This model is identical to that in Figure 6C with the addition of Atg8 (light orange and orange) thiolester linked to Atg7's catalytic cysteines. Atg7 and Atg3 catalytic cysteines are shown as green spheres.

SUPPLEMENTAL REFERENCES

Adams, P.D., Afonine, P.V., Bunkoczi, G., Chen, V.B., Davis, I.W., Echols, N., Headd, J.J., Hung, L.W., Kapral, G.J., Grosse-Kunstleve, R.W.*, et al.* (2010). PHENIX: a comprehensive Python-based system for macromolecular structure solution. Acta Crystallogr D Biol Crystallogr *66*, 213-221.

Baker, N.A., Sept, D., Joseph, S., Holst, M.J., and McCammon, J.A. (2001). Electrostatics of nanosystems: application to microtubules and the ribosome. Proc Natl Acad Sci U S A *98*, 10037-10041.

Bolanos-Garcia, V.M., and Davies, O.R. (2006). Structural analysis and classification of native proteins from E. coli commonly co-purified by immobilised metal affinity chromatography. Biochim Biophys Acta *1760*, 1304-1313.

Emsley, P., Lohkamp, B., Scott, W.G., and Cowtan, K. (2010). Features and development of Coot. Acta Crystallogr D Biol Crystallogr *66*, 486-501.

Franke, D., and Svergun, D.I. (2009). DAMMIF, a program for rapid ab-initio shape determination in small-angle scattering. Journal of Applied Crystallography *42*, 342-346.

Guinier, A., and Fournet, F. (1955). Small Angle Scattering of X-rays. (New York: Wiley Interscience).

Holm, L., and Rosenstrom, P. (2010). Dali server: conservation mapping in 3D. Nucleic Acids Res *38*, W545-549.

Hura, G.L., Menon, A.L., Hammel, M., Rambo, R.P., Poole, F.L., 2nd, Tsutakawa, S.E., Jenney, F.E., Jr., Classen, S., Frankel, K.A., Hopkins, R.C.*, et al.* (2009). Robust, high-throughput solution structural analyses by small angle X-ray scattering (SAXS). Nat Methods *6*, 606-612.

Ichimura, Y., Imamura, Y., Emoto, K., Umeda, M., Noda, T., and Ohsumi, Y. (2004). In vivo and in vitro reconstitution of Atg8 conjugation essential for autophagy. J Biol Chem *279*, 40584-40592.

Lake, M.W., Wuebbens, M.M., Rajagopalan, K.V., and Schindelin, H. (2001). Mechanism of ubiquitin activation revealed by the structure of a bacterial MoeB-MoaD complex. Nature *414*, 325-329.

Nakatogawa, H., Ichimura, Y., and Ohsumi, Y. (2007). Atg8, a ubiquitin-like protein required for autophagosome formation, mediates membrane tethering and hemifusion. Cell *130*, 165-178.

Noda, N.N., Fujioka, Y., Ohsumi, Y., and Inagaki, F. (2008a). Crystallization of the Atg12-Atg5 conjugate bound to Atg16 by the free-interface diffusion method. J Synchrotron Radiat *15*, 266-268.

Noda, N.N., Kumeta, H., Nakatogawa, H., Satoo, K., Adachi, W., Ishii, J., Fujioka, Y., Ohsumi, Y., and Inagaki, F. (2008b). Structural basis of target recognition by Atg8/LC3 during selective autophagy. Genes Cells *13*, 1211-1218.

Pelikan, M., Hura, G.L., and Hammel, M. (2009). Structure and flexibility within proteins as identified through small angle X-ray scattering. Gen Physiol Biophys *28*, 174-189.

Pena, V., Liu, S., Bujnicki, J.M., Luhrmann, R., and Wahl, M.C. (2007). Structure of a multipartite protein-protein interaction domain in splicing factor prp8 and its link to retinitis pigmentosa. Mol Cell *25*, 615-624.

Sanches, M., Alves, B.S., Zanchin, N.I., and Guimaraes, B.G. (2007). The crystal structure of the human Mov34 MPN domain reveals a metal-free dimer. J Mol Biol *370*, 846-855.

Sanjuan, M.A., Dillon, C.P., Tait, S.W., Moshiach, S., Dorsey, F., Connell, S., Komatsu, M., Tanaka, K., Cleveland, J.L., Withoff, S., and Green, D.R. (2007). Toll-like receptor signalling in macrophages links the autophagy pathway to phagocytosis. Nature *450*, 1253-1257.

Sato, Y., Yoshikawa, A., Yamagata, A., Mimura, H., Yamashita, M., Ookata, K., Nureki, O., Iwai, K., Komada, M., and Fukai, S. (2008). Structural basis for specific cleavage of Lys 63-linked polyubiquitin chains. Nature *455*, 358-362.

Schneidman-Duhovny, D., Hammel, M., and Sali, A. (2010). FoXS: a web server for rapid computation and fitting of SAXS profiles. Nucleic Acids Res *38*, W540-544.

Schuck, P. (2000). Size-distribution analysis of macromolecules by sedimentation velocity ultracentrifugation and lamm equation modeling. Biophys J *78*, 1606-1619.

Schuck, P., Perugini, M.A., Gonzales, N.R., Howlett, G.J., and Schubert, D. (2002). Size-distribution analysis of proteins by analytical ultracentrifugation: strategies and application to model systems. Biophys J *82*, 1096-1111.

Tran, H.J., Allen, M.D., Lowe, J., and Bycroft, M. (2003). Structure of the Jab1/MPN domain and its implications for proteasome function. Biochemistry *42*, 11460-11465.

Vistica, J., Dam, J., Balbo, A., Yikilmaz, E., Mariuzza, R.A., Rouault, T.A., and Schuck, P. (2004). Sedimentation equilibrium analysis of protein interactions with global implicit mass conservation constraints and systematic noise decomposition. Anal Biochem *326*, 234-256.

Werner, A.B., de Vries, E., Tait, S.W., Bontjer, I., and Borst, J. (2002). TRAIL receptor and CD95 signal to mitochondria via FADD, caspase-8/10, Bid, and Bax but differentially regulate events downstream from truncated Bid. J Biol Chem *277*, 40760-40767.

Yamada, Y., Suzuki, N.N., Hanada, T., Ichimura, Y., Kumeta, H., Fujioka, Y., Ohsumi, Y., and Inagaki, F. (2007). The crystal structure of Atg3, an autophagy-related ubiquitin carrier protein (E2) enzyme that mediates Atg8 lipidation. J Biol Chem *282*, 8036-8043.